ACS APPLIED MATERIALS & INTERFACES

www.acsami.org Research Article

Quantifying Image Charge Effects in Molecular Tunnel Junctions Based on Self-Assembled Monolayers of Substituted Oligophenylene Ethynylene Dithiols

Zuoti Xie,*,# Valentin Diez Cabanes,# Quyen Van Nguyen, Sandra Rodriguez-Gonzalez, Lucie Norel, Olivier Galangau, Stéphane Rigaut, Jérôme Cornil,* and C. Daniel Frisbie*

Cite This: *ACS Appl. Mater. Interfaces* 2021, 13, 56404−56412 Read Online

ACCESS | Metrics & More | Article Recommendations | Supporting Information

ABSTRACT: A number of factors contribute to orbital energy alignment with respect to the Fermi level in molecular tunnel junctions. Here, we report a combined experimental and theoretical effort to quantify the effect of metal image potentials on the highest occupied molecular orbital to Fermi level offset, ε_h, for molecular junctions based on self-assembled monolayers (SAMs) of oligophenylene ethynylene dithiols (OPX) on Au. Our experimental approach involves the use of both transport and photoelectron spectroscopy to extract the offsets, ε_h^{trans} and ε_h^{UPS}, respectively. We take the difference in these quantities to be the image potential energy eV_{image}. In the theoretical approach, we use density functional theory (DFT) to calculate directly eV_{image} between positive charge on an OPX molecule and the negative image charge in the Au. Both approaches yield $eV_{image} \sim -0.1$ eV per metal contact, meaning that the total image potential energy is ∼−0.2 eV for an assembled junction with two Au contacts. Thus, we find that the total image potential energy is 25−30% of the total offset ε_h, which means that image charge effects are significant in OPX junctions. Our methods should be generally applicable to understanding image charge effects as a function of molecular size, for example, in a variety of SAM-based junctions.

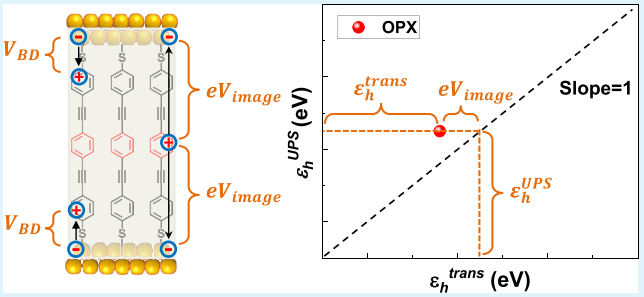

KEYWORDS: *molecular junction, tunneling, charge transport, image charge, Fermi level-HOMO offset, single level model, photoelectron spectroscopy*

INTRODUCTION

Relating the conductance behavior of molecules to their electronic structure is a central focus of the field of molecular electronics.[1−20] However, electronic phenomena at the interface between discrete molecules and metal electrodes generally yield substantial changes in orbital energies with respect to their values in isolated molecules, and thus, understanding these factors is critical. The presence of metal−molecule bond dipoles and metal image potentials are two recognized effects responsible for shifting of orbital energies when a molecule binds to a metallic substrate.[21−32] Additionally, for junctions based on molecular assemblies such as self-assembled monolayers (SAMs) rather than single molecules, intermolecular interactions also play a major role in energy level alignment.[28]

In this paper, we seek additional clarity on factors affecting orbital energies in junctions based on SAMs of an oligophenylene ethynylene (OPE) dithiol[33−37] and substituted derivatives (OPX = OPM, OPF, and OPN) on Au, as shown in Figure 1A,B. The original design principle underlying the OPX system was to exploit electroactive donating and withdrawing substituents on the central ring to manipulate the orbital level alignment. However, we have previously demonstrated a pronounced highest-occupied molecular orbital (HOMO) level pinning in molecular junctions based on three of these molecules, OPE, OPF, and OPN.[28] The HOMO pinning, which appears to be a general phenomenon in molecules strongly coupled to metal electrodes,[26,38−45] is striking, as OPE, OPF, and OPN have gas-phase (isolated molecule) ionization energies E_I that differ by over 0.6 eV due to the different electroactive substituents on the central ring. Density functional theory (DFT) calculations reveal that the differences in E_I are nearly completely wiped out in crystalline monolayers of OPE, OPF, and OPN due to intermolecular interactions (specifically electrostatic interactions); the ionization potentials (IPs) for the three monolayers are approximately equal.[28] Thus, intermolecular interactions play a

Received: August 26, 2021
Accepted: November 2, 2021
Published: November 16, 2021

https://doi.org/10.1021/acsami.1c16398
ACS Appl. Mater. Interfaces 2021, 13, 56404−56412

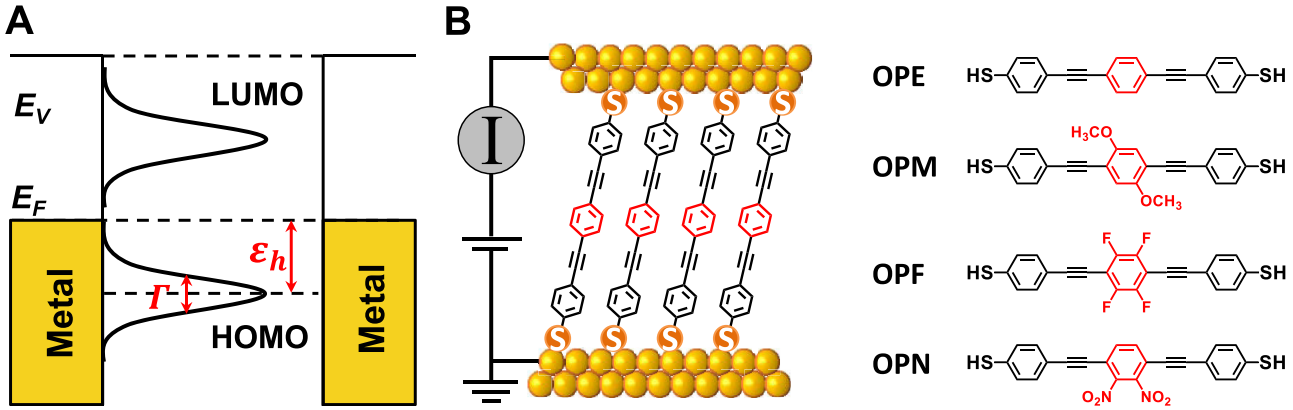

Figure 1. (A) Typical electronic structure of a molecular junction with key parameters ε_h and Γ and (B) Schematic representation of the molecular junctions based on OPE, OPM, OPF, and OPN with Au electrodes.

substantial role in the HOMO pinning and energy level alignment that occurs in close-packed OPX monolayers contacted by metal electrodes. We know from our prior theoretical work that the Au−S bond dipoles are also critical to energy level alignment in these systems,[46] but they are nearly equal across all the OPX derivatives in SAMs.[27,28]

For molecules such as the OPX series where the bond dipoles at either contact are noninteracting (see Results and Discussion), the spectra of effects impacting orbital energies in molecular junctions are approximately independent. In such a case, one can write that the HOMO position ε_h with respect to the Fermi level E_f is the sum of four contributions

$$\varepsilon_h + E_f = E_I + \Delta E_{I\_intermolecular} + BD + eV_{image} \quad (1)$$

where E_I is the IP of the isolated molecule, $\Delta E_{I\_intermolecular}$ is the shift in E_I due to intermolecular interactions in a SAM, BD is the energy shift due to the molecule−metal bond that induces the bond dipole,[21,22] e is the elementary charge, and V_{image} is the image potential associated with the metal electrodes.[29,30] Please note that in eq 1, ε_h and E_f are taken as positive quantities simply for convenience ($\varepsilon_h > 0$ is typical in molecular electronics), though in formal electron energy level diagrams, they would both be negative of the vacuum level $E_v = 0$ (Figure 1). With the sign convention used here, $eV_{image} < 0$ reduces, ε_h, that is, shifts the HOMO upward.

It is also critical to note that the absolute magnitude of V_{image} is anticipated to scale with the number of metal contacts, that is, V_{image} for a SAM-based molecular junction with two metal contacts is expected to be approximately twice as large as V_{image} for a SAM on a metal substrate (i.e., with one contact), as long as the relevant transport orbital (e.g., HOMO) is relatively spatially symmetric within the junction. In contrast, E_I and $\Delta E_{I\_intermolecular}$ do not depend on the number (or presence) of contacts, and BD, as we will explain below, is approximately the same for one vs. two metal contacts. The significance of this is described shortly.

Here, our particular focus is on determining the role of the image potential V_{image} on orbital energies in OPX molecular junctions. Ionization energies and electron affinities (EAs) of molecules near metal surfaces can be profoundly affected by the metal's image potential,[23,24,29−32] and this in turn can influence the HOMO (or LUMO) alignment with respect to the Fermi level. However, these effects depend on the proximity of the molecule to the metal surface and, crucially, on molecular orientation with respect to the surface.[47−49] It is not immediately clear how big the image charge effect will be for a given molecular junction.

In this paper, we estimate V_{image} experimentally and theoretically. Our experimental approach involves extraction of the HOMO to Fermi level offset, ε_h^{trans}, from current−voltage (I−V) measurements on Au−OPX−Au junctions and subsequent comparison with ε_h^{UPS} for OPX SAMs on Au obtained by ultraviolet photoelectron spectroscopy (UPS). The transport measurement involves two contacts to the SAM, while UPS probes the OPX SAM on one metal contact. Thus, ε_h^{trans} is the experimental estimation of ε_h shown in Figure 1A from transport measurements, and ε_h^{UPS} is the corresponding experimental value of ε_h for a SAM (one contact) obtained by UPS. As noted above, because to a first approximation only eV_{image} on the right hand side of eq 1 depends on the number of contacts, we can employ the difference between ε_h^{trans} and ε_h^{UPS} to provide an estimate of the image charge effect due to the second contact, that is, $eV_{image} = \varepsilon_h^{trans} - \varepsilon_h^{UPS}$.

Our theoretical approach to V_{image} begins with DFT calculations of the electronic structure of a neutral junction to evaluate the relative location of the HOMO levels of the OPX derivatives with respect to the Fermi level of Au. The image charge effect is then estimated in a second step by first mirroring the distribution of the positive charge over the OPX backbone with respect to the metal surface and then by computing the Coulomb interaction between the two distributions of opposite sign; this is achieved by making the reasonable assumption that the interface dipole and the image charge have a weak mutual influence. Importantly, both experiments and theory demonstrate the image potential contribution to ε_h to be ∼0.1 eV per contact for OPX, which translates to approximately 25−30% of the total magnitude of ε_h for complete, two-contact junctions. Note that this significant effect differs slightly from previous findings in which the image charge in single molecule junctions was found to dominate the energy level alignment.[23,24,29−32] Our results do not contradict the earlier findings, but rather indicate that image charge effects are system-specific and depend on the size and orientation of molecules with respect to the metal electrodes, as well as the electrode shape and total number of electrodes (up to 3 if there is a gate).

In summary, we present an experimental approach using junction conductance measurements and photoelectron spectroscopy to quantify image charge effects. The results are verified theoretically and are important for developing a

https://doi.org/10.1021/acsami.1c16398
ACS Appl. Mater. Interfaces 2021, 13, 56404−56412

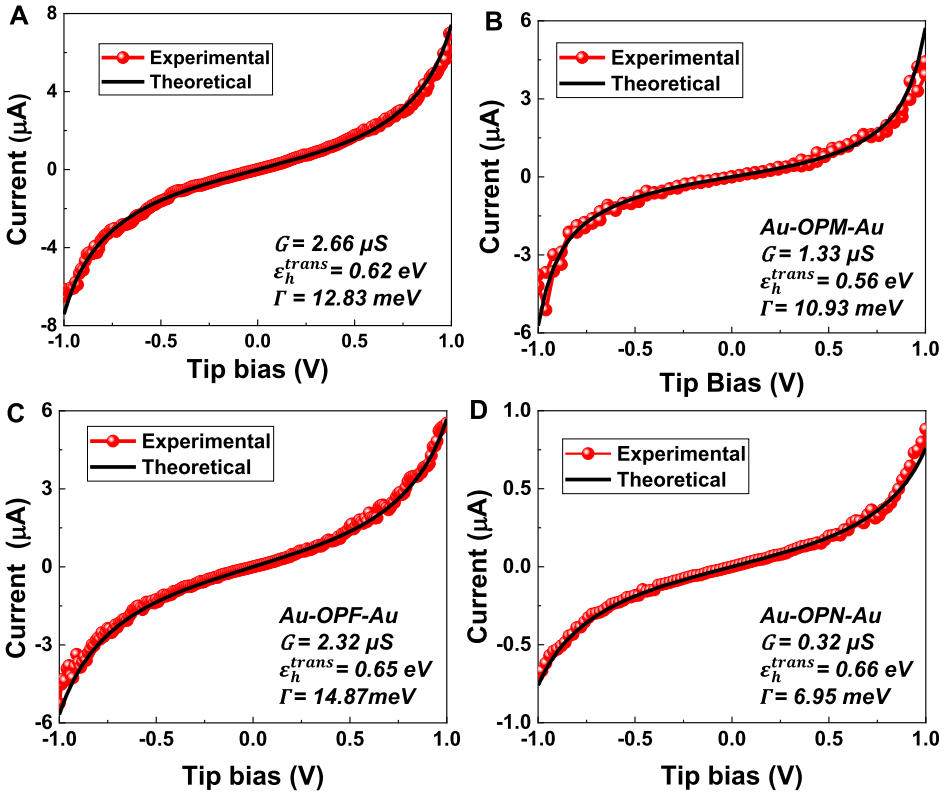

Figure 2. Experimental $I-V$ curves (red) and single level model simulations via eq 2 (black) for (A) Au−OPE−Au, (B) Au−OPM−Au, (C) Au−OPF−Au, and (D) Au−OPN−Au junctions. The three extracted parameters for each junction, that is, low bias conductance G ($1/R$), the energy offset ε_h^{trans}, and coupling Γ, are listed in each panel. The N values used for calculating Γ are 80, 45, 55, and 35 for OPE, OPM, OPF, and OPN, respectively.

comprehensive picture of factors impacting energy level alignment in SAM-based molecular junctions.

METHODS

Materials. Gold nuggets (99.999% pure) were purchased from Mowrey, Inc. (St. Paul, MN). Evaporation boats and chromium evaporation rods were purchased from R. D. Mathis (Long Beach, CA). Silicon (100) wafers were obtained from WaferNet (San Jose, CA). Contact mode AFM tips (DNP SiN probes) were purchased from Bruker AFM Probes. The synthesis of the three-ring OPE and substituted derivatives (OPF and OPN) has been described elsewhere.[50,51] The synthesis of OPM is described in Section S1 in Supporting Information.

Monolayer Growth and Characterization. Preparation of conducting tips and template-stripped flat Au substrates is described in a previous publication.[42] SAMs were formed by immersing clean template-stripped flat metal substrates into ethanol solutions of the molecules at a concentration of ∼1 mM for 20 h. The thicknesses of the OPE, OPM, OPF, and OPN SAMs were characterized by ellipsometry (Figure S1) carried out on a VASE spectroscopic ellipsometer (J. A. Woolam Co., Inc). The extracted molecular tilt angles from the normal direction amount to 33, 34, 30, and 34° for OPE, OPM, OPF, and OPN, respectively. The X-ray photoelectron spectroscopy (XPS) was used to characterize the difference of the surface coverage of SAMs (Figure S2) and the UPS was used to measure the HOMO-Fermi level offset of OPE, OPM, OPF, and OPN SAMs on the Au substrate. More details about XPS and UPS are described in Supporting Information.

Transport Measurements. Current−voltage measurements were completed by mounting the substrates in the AFM and bringing the metal coated tip into contact with the SAM under ∼1 nN of applied compressive load. Voltages were applied to the tip with a Keithley model 236 source-measure unit operated in "DC mode". Voltage was swept at the tip, with the bottom substrate grounded, and current−voltage characteristics ($I-V$) were recorded ($V > 0$ corresponds to a positive voltage on the tip). All measured $I-V$ curves (about 100 curves were collected for each OPX junction) crossed over from practically linear at low biases to gradually more nonlinear at higher biases. The inverse of the slope of the linear portion of the $I-V$ characteristic was used to define a junction resistance R at low bias. Voltage sweeps to ±1.2 V were applied to observe the pronounced nonlinear ($I-V$) behavior.

Theoretical Calculations. The methodology used to model the SAMs is the same as that used in our previous work.[28] Additional information related with the computational details and the models employed to simulate the OPE-based SAMs and junctions are provided in Section S2 of the Supporting Information.

RESULTS AND DISCUSSION

Analysis of Transport Characteristics; Extraction of ε_h^{trans}. Figure 2 shows representative $I-V$ characteristics for junctions based on OPX SAMs with Au contacts; such a complete dataset was not shown in our prior publication.[28] To analyze these curves and to extract ε_h and the metal−molecule coupling Γ (see Figure 1), we employ the analytical single level model, which we have shown previously applies well to simple molecular tunnel junctions. In this model, the $I-V$ characteristics of a symmetric junction are given as[42,52]

$$I = GV\frac{\varepsilon_h^2}{\varepsilon_h^2 - (eV/2)^2} \quad (2)$$

where the zero-bias conductance G of the junction can be expressed as follows

https://doi.org/10.1021/acsami.1c16398
ACS Appl. Mater. Interfaces 2021, 13, 56404−56412

Table 1. Summary of the Experimental Results, Including Low Bias Conductance of the Junctions G, Estimated Conductance per Molecule G_m, Relative Difference in Molecular Coverage A, Energy Offset ε_h^{trans}, and Average Coupling Γ for the Junctions Made with SAMs of the OPE derivatives[a]

quantity	OPE	OPM	OPF	OPN
G	$(3.00 \pm 0.71) \times 10^{-6}$	$(2.20 \pm 0.50) \times 10^{-6}$	$(2.56 \pm 0.62) \times 10^{-6}$	$(0.31 \pm 0.11) \times 10^{-6}$
A	1	0.57	0.69	0.43
G_m	$(3.75 \pm 0.88) \times 10^{-8}$	$(4.80 \pm 1.09) \times 10^{-8}$	$(4.66 \pm 1.12) \times 10^{-8}$	$(0.87 \pm 0.33) \times 10^{-9}$
ε_h^{trans}	0.61 ± 0.06	0.56 ± 0.07	0.63 ± 0.07	0.67 ± 0.1
ε_h^{UPS}	0.68 ± 0.1	0.65 ± 0.1	0.71 ± 0.1	0.74 ± 0.1
Γ_{av}	13.42 ± 2.20	13.94 ± 2.01	15.44 ± 2.75	7.09 ± 1.51

[a] ε_h^{UPS} is the Fermi-HOMO offset of the OPE-based SAMs obtained by UPS. Units: G in S, V_t in V, ε_h in eV, and Γ in meV obtained from eq 3 by taking $N = 80$ for OPE as the reference junction[55] and $N = 45$, 55, and 35 for OPM, OPF, and OPN, respectively. The averaged results from transport measurements were obtained from approximately 100 $I-V$ curves for each OPX SAM.

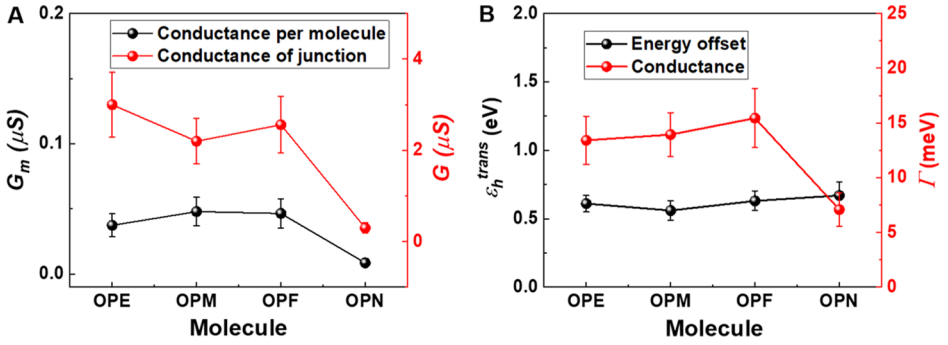

Figure 3. Plots of the comparison between (A) low bias conductance per molecule G_m and junction conductance G and (B) energy offset ε_h^{trans} and coupling Γ for OPE, OPM, OPF, and OPN junctions.

$$G = NG_0\frac{\Gamma^2}{\varepsilon_h^{\,2}} \tag{3}$$

In eq 3, $\Gamma = \sqrt{\Gamma_s\Gamma_t} = \varepsilon_h\sqrt{G/NG_0}$ is the average interface coupling; Γ_s and Γ_t are determined by the molecular coupling to the substrate (s) and tip (t) ($\Gamma_s \approx \Gamma_t$ in symmetric junctions), $G_0 = 2e^2/h$ is the quantum conductance, and N is the number of molecules participating in the transport.

We have used eq 2 to fit the data in Figure 2 (see Supporting Information for the fitting method). Doing so, we reproduce the individual measured $I-V$ curves for the OPX junctions extremely well, as shown by the black traces in Figure 2. We believe that the very good match between the experimental and simulated $I-V$ curves indicates that the single level model applies well for OPX-based molecular junctions, as we have shown for other molecular systems.[41−45,53,54]

The average values for the transport parameters extracted from approximately 100 $I-V$ curves for each type of OPX SAM are compiled in Table 1. Evidently, substitution of the central ring with electron donating or withdrawing groups does influence the low bias conductance G of the OPX molecular junctions, but not to a large extent. Because substitution introduces steric interactions in the SAMs resulting in variations in the molecular packing density, the differences in molecular surface coverage across the OPX series were estimated by XPS (Figure S2). The C_{1s} signal normalized to the Au_{4f} signal for each OPX derivative was employed to calculate the relative surface coverage A of the SAMs; values of A are listed in Table 1. After correction for surface coverage, the conductance $G_m = G/N$ per molecule also shows modest variation among the substituted OPX molecules. Figure 3A depicts the G and G_m data graphically and indeed only the OPN system appears to be appreciably different.

The estimated energy offsets ε_h^{trans} and interface couplings Γ extracted from the transport data are also listed in Table 1 and they are plotted in Figure 3B. It is evident that ε_h^{trans} is essentially invariant across the OPX species, which is the signature of HOMO level pinning in molecular junctions.[28,42] Again, this is striking because the electron donating (OPM) and electron withdrawing (OPF and OPN) substituents on the central phenylene ring can shift the IP by as much as 0.6 eV for isolated (gas phase) OPX molecules.[28] Comparison of Figure 3A,B reveals that the weak dependence of the energy offset ε_h^{trans} on the electroactive substituents cannot explain the much larger (by one order of magnitude) difference in conductance G_m between OPN and the other OPX molecules (OPE, OPM, and OPF). The cause of the conductance difference for OPN is Γ, which, as shown in Figure 3B, is significantly lower for OPN than for the other molecules. Note that $G \propto \Gamma^2$ via eq 3. Given the very similar ε_h^{trans} values for the OPX junctions, the larger drop of the coupling (as well as the conductance) obtained for OPN is tentatively attributed to stronger localization of the HOMO level over the central ring, thus limiting the electrode−molecular interfacial coupling and hence the efficiency of charge transport.[28]

Measurement of ε_h^{UPS} and Estimation of the Image Charge Potential V_{image}. UPS is the standard experimental method used to obtain the energy of the HOMO for molecular thin films.[44,56−58] To obtain an independent verification of the energy level alignment ε_h^{trans} extracted from transport measurements and to understand the influence of the top electrode on ε_h, that is, to estimate the image charge effect, we performed UPS on each OPX SAM. The spectra for OPE, OPM, OPF, and OPN SAMs on Au substrates are shown in Supporting Information, Figure S3. In these UPS spectra, the Fermi edge at zero binding energy is clearly evident and the HOMO-Fermi

https://doi.org/10.1021/acsami.1c16398
ACS Appl. Mater. Interfaces 2021, 13, 56404−56412

level offsets are determined using standard extrapolation protocols.[59,60] The resulting ε_h^{UPS} values obtained by UPS are then compared to the corresponding ε_h^{trans} values obtained from transport data, as shown in Figure 4 and Table 1. It is clear in

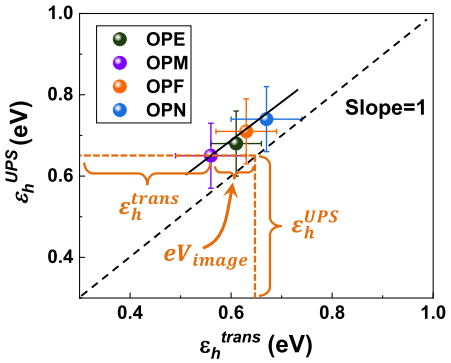

Figure 4. Correlation of ε_h^{trans} extracted from transport measurements (and the single level model) with ε_h^{UPS} from UPS measurements on SAMs for OPE, OPM, OPF, and OPN with Au contacts. The black dashed line shows the slope = 1 trend for perfect correspondence, and the black solid line shows the linear fit.

both Table 1 and Figure 4 that $\varepsilon_h^{trans}$is systematically less than ε_h^{UPS} for each OPX molecule. This immediately implies an upward energy level shift of the OPX HOMOs in the two-contact molecular junctions versus the one-contact SAMs, that is, $eV_{image} < 0$, where $eV_{image} \approx \varepsilon_h^{trans} - \varepsilon_h^{UPS}$. This result is consistent with expectations because the image charge stabilization should be additive, that is, greater (roughly twice the size) for two contacts than for one contact. Importantly, ε_h^{UPS} also scales linearly with ε_h^{trans} as shown by the fit to the data in Figure 4 with a slope = 0.9. The linear correlation with a slope ∼1 is important in two respects. First, it is consistent with the straightforward interpretation that eV_{image} is the only term that changes in eq 1 when comparing OPX SAMs vs. OPX junctions. If the data were not linear with slope ∼1, we would be forced to conclude that either the value of eV_{image} was different for each OPX molecule when adding a second contact (which is not supported by theory, nor expected, see below) or that the BD term for each OPX molecule was different in the two-contact junctions versus the one-contact SAM. Second, we note that there is significant uncertainty associated with individual values of $\varepsilon_h^{trans}$and ε_h^{UPS} for any given OPX molecule, as indicated by the error bars in Figure 4. However, the four measurements on four molecules minimize the overall error. From the four measurements, we conclude that $eV_{image} = -0.08 \pm 0.01$ eV for the OPX system.

As just noted, the bond dipole energy BD in eq 1 is not influenced by whether there are one or two contacts to an OPX SAM. A second bond dipole likely forms when the top contact is made to an OPX SAM, but it does not lead to a change in ε_h^{trans}. This is because the charge transfer is localized at the contact and the vacuum level shift associated with the dipole is the mirror image of the shift at the first contact. This point is discussed further in the theory section. Note that the independence of BD on the number of contacts is a very different conclusion than we made about eV_{image}, which is expected to scale with the number of contacts because of the longer range of the charge-metal interaction that underlies the image charge effect, and the fact that the HOMO is symmetrically distributed in the junction.

We conclude from our experimental measurements that eV_{image} associated with a single contact is ∼−0.08 eV for SAM-based OPX junctions. Given that the total energy level offset ε_h^{trans} is ∼0.6 eV, eV_{image} is clearly important as each contact provides ∼−0.08 eV, meaning that the total contribution of eV_{image} to ε_h^{trans} is ∼−0.16 eV or 25% of the total offset from E_f. One can say that image charge effects are a significant factor—though not the dominant factor—in overall energy alignment in OPX junctions.[23,24,29−32]

We next compare the experimental data to DFT calculations. Specifically, we are able to assess the role of interfacial charge transfer and the resulting Au−S bond dipoles, which determine BD. We also explicitly estimate eV_{image}.

DFT Calculations. Theoretical results for OPE, OPF, and OPN SAM-based junctions have been reported in a previous paper[28] and that previous study has been extended here to consider OPM and eV_{image} explicitly. Because the HOMO energy offset appears experimentally to be weakly affected by the actual areal density of the OPX derivatives, the SAMs were optimized with the same unit cell for each derivative, while imposing that the S atom is anchored on a Au bridge site and that the orientation of the backbone is normal to the surface (Figure S5); the latter constraint is motivated by the fact that the measured tilt angles are moderate and similar for all OPX compounds. The full theoretical methodology is described in ref 28. Table 2 collects the calculated HOMO offsets with

Table 2. Summary of the DFT Calculated Energy Offset $\varepsilon_{h,DFT}^{SAM}$ and $\varepsilon_{h,DFT}^{junction}$ in SAMs and Molecular Junctions, Respectively, and Amplitudes of the Image Charge Energies (eV_{IP} and eV_{EA}) Calculated for the IP and EA. All Values are Given in eV.

quantity	OPE	OPM	OPF	OPN
$\varepsilon_{h,DFT}^{SAM}$	0.61	0.63	0.64	0.65
$\varepsilon_{h,DFT}^{junction}$	0.54	0.56	0.56	0.59
eV_{image}^{IP}	−0.11	−0.11	−0.13	−0.14
eV_{image}^{EA}	0.13	0.13	0.12	0.12

respect to the Fermi level in one-contact OPX SAMs ($\varepsilon_{h,DFT}^{SAM}$) and two-contact molecular junctions ($\varepsilon_{h,DFT}^{Junction}$). Note that these values are extracted from the density of states of the SAM (central scattering region of the junction) projected onto C atoms as the energy at the maximum of the first intense band below the Fermi level (see Figures S8 and S9). The calculated ε_h values appear to be in quite good quantitative agreement with the corresponding experimental transport and UPS results, as shown in Figure 5A,B, in spite of the well-known limitations of DFT approaches in accurately predicting the energetic level alignment at hybrid interfaces. This can be qualitatively explained by a compensation error between the underestimation of the HOMO−LUMO gap of isolated molecules at the DFT/GGA level versus the neglect of electronic polarization effects in the solid state (due to the presence of electrodes and neighboring molecules) that strongly reduce the gap of isolated molecules (no explicit charge is considered when computing transmission spectra within the DFT/NEGF approach).[61]

Importantly, the DFT calculations show that anchoring the SAMs on Au or introducing a second Au slab to build up the junction (Figure S6) promotes a small charge transfer at each interface (between 0.12 and 0.14 lel, Figure S7), as computed using either the Hirschfeld or Voronoi charge population

https://doi.org/10.1021/acsami.1c16398
ACS Appl. Mater. Interfaces 2021, 13, 56404−56412

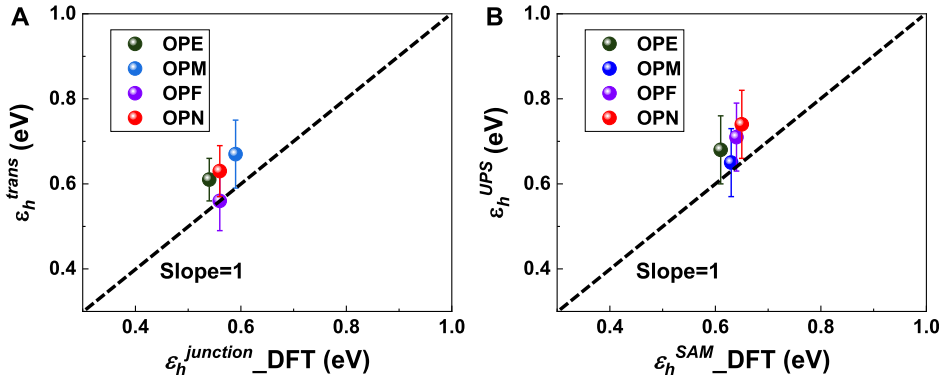

Figure 5. (A) Correlation of ε_h^{trans} from transport measurements (and the single level model) with DFT calculated energy offsets $\varepsilon_{h\_DFT}^{junction}$ for SAM-based junctions of OPE, OPM, OPF, and OPN with two Au contacts. (B) Correlation of ε_h^{UPS} from UPS measurements with the DFT calculated energy offsets $\varepsilon_{h\_DFT}^{SAM}$ for OPE, OPM, OPF, and OPN SAMs on an Au substrate.

analysis (Table S1). The bond dipoles are symmetric (they point in opposite directions) and their associated electrostatic potentials, centered at each end of the OPX molecules, weakly overlap, and this means that the alignment of the HOMO level is controlled by a single electrode. In other words, the formation of a second bond dipole at the second Au contact/SAM interface does not produce an additional electrostatic energy shift BD of the HOMO level (see eq 1). This is nicely demonstrated in Figure 6, which shows the planar averaged

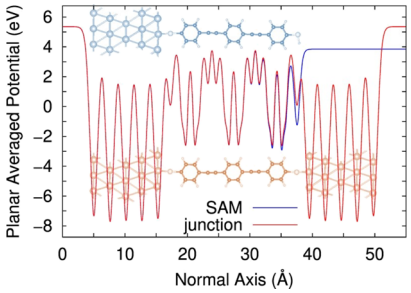

Figure 6. Calculated planar averaged potential in the Au/SAM vs Au/SAM/Au systems involving OPE, pointing to the weak coupling between the bond dipoles in the junction in view of the similar energy profile over the molecular backbone.

electrostatic potential across the Au/SAM and Au/SAM/Au systems involving OPE, highlighting the identical profile over the backbone and hence the independent character of the bond dipoles. BD is thus determined by one contact, that is, by the formation of the SAMs on Au.[13] This is a crucial conclusion, because as discussed in the Introduction, only eV_{image} on the right hand side of eq 1 depends on the number of contacts, which allows us to estimate eV_{image} from the difference in experimental two-contact versus one-contact ε_h values, $eV_{image} \approx \varepsilon_h^{trans} - \varepsilon_h^{UPS}$.

In order to calculate eV_{image} theoretically, taking the difference between computed $\varepsilon_{h,DFT}^{Junction}$ and $\varepsilon_{h,DFT}^{SAM}$ values—in analogy with the experimental approach—is not valid, as the DFT-NEGF calculations described so far were performed on neutral systems; they do not take into account the influence of electronic polarization, due both to the creation of an image potential in the metallic electrode when a molecule is charged and to induced dipoles in molecules surrounding the charged molecule. Thus, eV_{image} has been explicitly calculated here for one electrode as the interaction energy between the distribution of a positive charge over a molecule and its image (see Supporting Information for further details). We find that it leads to a shift of the IP and EA for all OPX compounds. The computed values of eV_{image}^{IP} and eV_{image}^{EA} reported in Table 2 are obtained with the RO(MP2) approach and are consistent with those previously computed for oligophenylene molecules.[27] They are also independent of the level of theory employed (Table S2) and of the molecular tilt angle (Table S3) and typically range between −0.11 and −0.14 eV, which is in good agreement with eV_{image} estimated from experiments. Thus, the DFT results support the conclusion that image effects are significant, but not dominant, in OPX junctions. Before closing this part, we note that our theoretical model used to estimate the image potentials neglects cooperative effects between neighboring molecules within the SAM that might lead to some depolarization effects.[62] Nevertheless, it provides a first approximation to the magnitude of the image effect associated with one electrode, and it verifies that the chemical substituents on the OPX core do not significantly influence the magnitude of the potential.

CONCLUSIONS

Through a combination of experiments and quantum chemical calculations, we have investigated the magnitude of the image charge effect on the HOMO energy offsets in molecular junctions based on SAMs of a series of OPX molecules on Au. On the experimental side, we have proposed that the image potential energy eV_{image} can be estimated by taking the difference between the HOMO level offset determined from transport measurements, ε_h^{trans}, and the offset determined by UPS, ε_h^{UPS}, that is, $eV_{image} \approx \varepsilon_h^{trans} - \varepsilon_h^{UPS}$. Using that approach, we find that eV_{image} is −0.08 ± 0.01 eV per metal contact, so that the total contribution of eV_{image} to ε_h for a two contact junction is −0.16 eV or about 25% of the total offset. DFT calculations produce similar numbers for eV_{image}. We thus conclude that image charge effects are significant in OPX junctions and influence the overall energy level lineup. Furthermore, the combined experimental and theoretical approaches employed here should be applicable to other SAM-based junctions, allowing for the impact of image potentials to be assessed generally in SAM-based molecular junctions as a function of molecular orientation and length, for example.

https://doi.org/10.1021/acsami.1c16398
ACS Appl. Mater. Interfaces 2021, 13, 56404−56412

■ ASSOCIATED CONTENT

Supporting Information

The Supporting Information is available free of charge at https://pubs.acs.org/doi/10.1021/acsami.1c16398.

Experimental and theoretical details and supplementary tables and figures (PDF)

■ AUTHOR INFORMATION

Corresponding Authors

Zuoti Xie − *Department of Materials Science and Engineering, Guangdong Technion-Israel Institute of Technology, Shantou, Guangdong 515063, China; Department of Chemical Engineering and Materials Science, University of Minnesota, Minneapolis, Minnesota 55455, United States;* orcid.org/0000-0002-1828-0122; Email: zuoti.xie@gtiit.edu.cn

Jérôme Cornil − *Laboratory for Chemistry of Novel Materials, University of Mons, Mons B-7000, Belgium;* orcid.org/0000-0002-5479-4227; Email: edjerome.cornil@umons.ac.be

C. Daniel Frisbie − *Department of Chemical Engineering and Materials Science, University of Minnesota, Minneapolis, Minnesota 55455, United States;* orcid.org/0000-0002-4735-2228; Email: frisbie@umn.edu

Authors

Valentin Diez Cabanes − *Laboratory for Chemistry of Novel Materials, University of Mons, Mons B-7000, Belgium;* orcid.org/0000-0002-6234-2749

Quyen Van Nguyen − *Department of Chemical Engineering and Materials Science, University of Minnesota, Minneapolis, Minnesota 55455, United States;* orcid.org/0000-0003-0120-0971

Sandra Rodriguez-Gonzalez − *Laboratory for Chemistry of Novel Materials, University of Mons, Mons B-7000, Belgium; Department of Physical Chemistry, University of Malaga, Malaga 29071, Spain;* orcid.org/0000-0001-6563-7852

Lucie Norel − *Univ Rennes, CNRS, ISCR (Institut des Sciences Chimiques de Rennes)-UMR 6226, Rennes F-3500, France;* orcid.org/0000-0001-6654-1211

Olivier Galangau − *Univ Rennes, CNRS, ISCR (Institut des Sciences Chimiques de Rennes)-UMR 6226, Rennes F-3500, France;* orcid.org/0000-0002-1952-6585

Stéphane Rigaut − *Univ Rennes, CNRS, ISCR (Institut des Sciences Chimiques de Rennes)-UMR 6226, Rennes F-3500, France;* orcid.org/0000-0001-7001-9039

Complete contact information is available at: https://pubs.acs.org/10.1021/acsami.1c16398

Author Contributions

#Z.X. and V.D.C. equal contribution.

Notes

The authors declare no competing financial interest.

■ ACKNOWLEDGMENTS

C.D.F. acknowledges financial support from the U.S. National Science Foundation (CHE-2003199). Parts of this work were carried out in the Characterization Facility, University of Minnesota, which receives partial support from NSF through the MRSEC program (DMR-2011401). The work of S.R.G. has been supported by the Belgian National Fund for Scientific Research (F.R.S.-FNRS). We also acknowledge the Consortium des Équipements de Calcul Intensif (CÉCI) funded by F.R.S.-FNRSfor providing the computational resources. J.C. is an FNRS research director.

■ REFERENCES

(1) Reed, M. A.; Zhou, C.; Muller, C. J.; Burgin, T. P.; Tour, J. M. Conductance of a Molecular Junction. *Science* **1997**, *278*, 252−254.

(2) Joachim, C.; Gimzewski, J. K.; Aviram, A. Electronics Using Hybrid-Molecular and Mono-Molecular Devices. *Nature* **2000**, *408*, 541−548.

(3) Ai, Y.; Kovalchuk, A.; Qiu, X.; Zhang, Y.; Kumar, S.; Wang, X.; Kühnel, M.; Nørgaard, K.; Chiechi, R. C. In-Place Modulation of Rectification in Tunneling Junctions Comprising Self-Assembled Monolayers. *Nano Lett.* **2018**, *18*, 7552−7559.

(4) Amdursky, N.; Marchak, D.; Sepunaru, L.; Pecht, I.; Sheves, M.; Cahen, D. Electronic Transport via Proteins. *Adv. Mater.* **2014**, *26*, 7142−7161.

(5) Li, Y.; Artés, J. M.; Demir, B.; Gokce, S.; Mohammad, H. M.; Alangari, M.; Anantram, M. P.; Oren, E. E.; Hihath, J. Detection and Identification of Genetic Material via Single-Molecule Conductance. *Nat. Nanotechnol.* **2018**, *13*, 1167−1173.

(6) Wang, K.; Vezzoli, A.; Grace, I. M.; McLaughlin, M.; Nichols, R. J.; Xu, B.; Lambert, C. J.; Higgins, S. J. Charge Transfer Complexation Boosts Molecular Conductance through Fermi Level Pinning. *Chem. Sci.* **2019**, *10*, 2396−2403.

(7) Lo, W.-Y.; Zhang, N.; Cai, Z.; Li, L.; Yu, L. Beyond Molecular Wires: Design Molecular Electronic Functions Based on Dipolar Effect. *Acc. Chem. Res.* **2016**, *49*, 1852−1863.

(8) Aragonès, A. C.; Haworth, N. L.; Darwish, N.; Ciampi, S.; Bloomfield, N. J.; Wallace, G. G.; Diez-Perez, I.; Coote, M. L. Electrostatic Catalysis of a Diels-Alder Reaction. *Nature* **2016**, *531*, 88−91.

(9) Yuan, L.; Wang, L.; Garrigues, A. R.; Jiang, L.; Annadata, H. V.; Anguera Antonana, M.; Barco, E.; Nijhuis, C. A. Transition from Direct to Inverted Charge Transport Marcus Regions in Molecular Junctions via Molecular Orbital Gating. *Nat. Nanotechnol.* **2018**, *13*, 322−329.

(10) Li, Y.; Buerkle, M.; Li, G.; Rostamian, A.; Wang, H.; Wang, Z.; Bowler, D. R.; Miyazaki, T.; Xiang, L.; Asai, Y.; Zhou, G.; Tao, N. Gate Controlling of Quantum Interference and Direct Observation of Anti-Resonances in Single Molecule Charge Transport. *Nat. Mater.* **2019**, *18*, 357−363.

(11) Liu, J.; Huang, X.; Wang, F.; Hong, W. Quantum Interference Effects in Charge Transport through Single-Molecule Junctions: Detection, Manipulation, and Application. *Acc. Chem. Res.* **2019**, *52*, 151−160.

(12) Xiang, D.; Wang, X.; Jia, C.; Lee, T.; Guo, X. Molecular-Scale Electronics: From Concept to Function. *Chem. Rev.* **2016**, *116*, 4318−4440.

(13) Nitzan, A.; Ratner, M. A. Electron Transport in Molecular Wire Junctions. *Science* **2003**, *300*, 1384−1389.

(14) Joachim, C.; Ratner, M. A. Molecular Electronics: Some Views on Transport Junctions and Beyond. *Proc. Natl. Acad. Sci. U.S.A.* **2005**, *102*, 8801−8808.

(15) Choi, S. H.; Kim, B. S.; Frisbie, C. D. Electrical Resistance of Long Conjugated Molecular Wires. *Science* **2008**, *320*, 1482−1486.

(16) Nijhuis, C. A.; Reus, W. F.; Siegel, A. C.; Whitesides, G. M. A Molecular Half-Wave Rectifier. *J. Am. Chem. Soc.* **2011**, *133*, 15397−15411.

(17) Park, S.; Wang, G.; Cho, B.; Kim, Y.; Song, S.; Ji, Y.; Yoon, M.-H.; Lee, T. Flexible Molecular-Scale Electronic Devices. *Nat. Nanotechnol.* **2012**, *7*, 438−442.

(18) Naaman, R.; Waldeck, D. H. Spintronics and Chirality: Spin Selectivity in Electron Transport through Chiral Molecules. *Annu. Rev. Phys. Chem.* **2015**, *66*, 263−281.

(19) Garner, M. H.; Li, H.; Chen, Y.; Su, T. A.; Shangguan, Z.; Paley, D. W.; Liu, T.; Ng, F.; Li, H.; Xiao, S.; Nuckolls, C.; Venkataraman, L.; Solomon, G. C. Comprehensive Suppression of Single-Molecule Conductance Using Destructive σ-Interference. *Nature* **2018**, *558*, 416−419.

(20) Xiang, L.; Hines, T.; Palma, J. L.; Lu, X.; Mujica, V.; Ratner, M. A.; Zhou, G.; Tao, N. Non-Exponential Length Dependence of Conductance in Iodide-Terminated Oligothiophene Single-Molecule Tunneling Junctions. *J. Am. Chem. Soc.* **2016**, *138*, 679−687.
(21) Heimel, G.; Romaner, L.; Brédas, J.-L.; Zojer, E. Interface Energetics and Level Alignment at Covalent Metal-Molecule Junctions: π-Conjugated Thiols on Gold. *Phys. Rev. Lett.* **2006**, *96*, 196806.
(22) Heimel, G.; Romaner, L.; Zojer, E.; Brédas, J.-L. Toward Control of the Metal−Organic Interfacial Electronic Structure in Molecular Electronics: A First-Principles Study on Self-Assembled Monolayers of π-Conjugated Molecules on Noble Metals. *Nano Lett.* **2007**, *7*, 932−940.
(23) Perrin, M. L.; Verzijl, C. J. O.; Martin, C. A.; Shaikh, A. J.; Eelkema, R.; Van Esch, J. H.; Van Ruitenbeek, J. M.; Thijssen, J. M.; Van Der Zant, H. S. J.; Dulić, D. Large Tunable Image-Charge Effects in Single-Molecule Junctions. *Nat. Nanotechnol.* **2013**, *8*, 282−287.
(24) Ivie, J. A.; Bamberger, N. D.; Parida, K. N.; Shepard, S.; Dyer, D.; Saraiva-Souza, A.; Himmelhuber, R.; McGrath, D. V.; Smeu, M.; Monti, O. L. A. Correlated Energy-Level Alignment Effects Determine Substituent-Tuned Single-Molecule Conductance. *ACS Appl. Mater. Interfaces* **2021**, *13*, 4267−4277.
(25) Schultz, T.; Lenz, T.; Kotadiya, N.; Heimel, G.; Glasser, G.; Berger, R.; Blom, P. W. M.; Amsalem, P.; de Leeuw, D. M.; Koch, N. Reliable Work Function Determination of Multicomponent Surfaces and Interfaces: The Role of Electrostatic Potentials in Ultraviolet Photoelectron Spectroscopy. *Adv. Mater. Interfaces* **2017**, *4*, 1700324.
(26) Kim, B.; Choi, S. H.; Zhu, X.-Y.; Frisbie, C. D. Molecular Tunnel Junctions Based on π-Conjugated Oligoacene Thiols and Dithiols between Ag, Au, and Pt Contacts: Effect of Surface Linking Group and Metal Work Function. *J. Am. Chem. Soc.* **2011**, *133*, 19864−19877.
(27) Diez-Cabanes, V.; Gonzalez, S. R.; Osella, S.; Cornil, D.; Van Dyck, C.; Cornil, J. Energy Level Alignment at Interfaces Between Au (111) and Thiolated Oligophenylenes of Increasing Chain Size: Theoretical Evidence of Pinning Effects. *Adv. Theory Simul.* **2018**, *1*, 1700020.
(28) Rodriguez-Gonzalez, S.; Xie, Z.; Galangau, O.; Selvanathan, P.; Norel, L.; Van Dyck, C.; Costuas, K.; Frisbie, C. D.; Rigaut, S.; Cornil, J. HOMO Level Pinning in Molecular Junctions: Joint Theoretical and Experimental Evidence. *J. Phys. Chem. Lett.* **2018**, *9*, 2394−2403.
(29) Lang, N. D.; Kohn, W. Theory of Metal Surfaces: Induced Surface Charge and Image Potential. *Phys. Rev. B: Solid State* **1973**, *7*, 3541−3550.
(30) Neaton, J. B.; Hybertsen, M. S.; Louie, S. G. Renormalization of Molecular Electronic Levels at Metal-Molecule Interfaces. *Phys. Rev. Lett.* **2006**, *97*, 216405.
(31) Quek, S. Y.; Choi, H. J.; Louie, S. G.; Neaton, J. B. Length Dependence of Conductance in Aromatic Single-Molecule Junctions. *Nano Lett.* **2009**, *9*, 3949−3953.
(32) Widawsky, J. R.; Darancet, P.; Neaton, J. B.; Venkataraman, L. Simultaneous Determination of Conductance and Thermopower of Single Molecule Junctions. *Nano Lett.* **2012**, *12*, 354−358.
(33) Huber, R.; González, M. T.; Wu, S.; Langer, M.; Grunder, S.; Horhoiu, V.; Mayor, M.; Bryce, M. R.; Wang, C.; Jitchati, R.; Schönenberger, C.; Calame, M. Electrical Conductance of Conjugated Oligomers at the Single Molecule Level. *J. Am. Chem. Soc.* **2008**, *130*, 1080−1084.
(34) Frisenda, R.; Stefani, D.; Van Der Zant, H. S. J. Quantum Transport through a Single Conjugated Rigid Molecule, a Mechanical Break Junction Study. *Acc. Chem. Res.* **2018**, *51*, 1359−1367.
(35) Stapleton, J. J.; Harder, P.; Daniel, T. A.; Reinard, M. D.; Yao, Y.; Price, D. W.; Tour, J. M.; Allara, D. L. Self-Assembled Oligo(Phenylene-Ethynylene) Molecular Electronic Switch Monolayers on Gold: Structures and Chemical Stability. *Langmuir* **2003**, *19*, 8245−8255.
(36) Kaliginedi, V.; Moreno-García, P.; Valkenier, H.; Hong, W.; García-Suárez, V. M.; Buiter, P.; Otten, J. L. H.; Hummelen, J. C.; Lambert, C. J.; Wandlowski, T. Correlations between Molecular Structure and Single-Junction Conductance: A Case Study with Oligo(Phenylene-Ethynylene)-Type Wires. *J. Am. Chem. Soc.* **2012**, *134*, 5262−5275.
(37) Liu, K.; Wang, X.; Wang, F. Probing Charge Transport of Ruthenium-Complex-Based Molecular Wires at the Single-Molecule Level. *ACS Nano* **2008**, *2*, 2315−2323.
(38) Sayed, S. Y.; Fereiro, J. A.; Yan, H.; McCreery, R. L.; Bergren, A. J. Charge Transport in Molecular Electronic Junctions: Compression of the Molecular Tunnel Barrier in the Strong Coupling Regime. *Proc. Natl. Acad. Sci. U.S.A.* **2012**, *109*, 11498−11503.
(39) Van Dyck, C.; Geskin, V.; Cornil, J. Fermi Level Pinning and Orbital Polarization Effects in Molecular Junctions: The Role of Metal Induced Gap States. *Adv. Funct. Mater.* **2014**, *24*, 6154−6165.
(40) Xie, Z.; Bâldea, I.; Frisbie, C. D. Why One Can Expect Large Rectification in Molecular Junctions Based on Alkane Monothiols and Why Rectification Is so Modest. *Chem. Sci.* **2018**, *9*, 4456−4467.
(41) Van Nguyen, Q. V.; Xie, Z.; Frisbie, C. D. Quantifying Molecular Structure-Tunneling Conductance Relationships: Oligophenylene Dimethanethiol vs Oligophenylene Dithiol Molecular Junctions. *J. Phys. Chem. C* **2021**, *125*, 4292−4298.
(42) Xie, Z.; Bâldea, I.; Smith, C. E.; Wu, Y.; Frisbie, C. D. Experimental and Theoretical Analysis of Nanotransport in Oligophenylene Dithiol Junctions as a Function of Molecular Length and Contact Work Function. *ACS Nano* **2015**, *9*, 8022−8036.
(43) Xie, Z.; Bâldea, I.; Frisbie, C. D. Energy Level Alignment in Molecular Tunnel Junctions by Transport and Spectroscopy: Self-Consistency for the Case of Alkyl Thiols and Dithiols on Ag, Au, and Pt Electrodes. *J. Am. Chem. Soc.* **2019**, *141*, 18182−18192.
(44) Xie, Z.; Bâldea, I.; Frisbie, C. D. Determination of Energy-Level Alignment in Molecular Tunnel Junctions by Transport and Spectroscopy: Self-Consistency for the Case of Oligophenylene Thiols and Dithiols on Ag, Au, and Pt Electrodes. *J. Am. Chem. Soc.* **2019**, *141*, 3670−3681.
(45) Smith, C. E.; Xie, Z.; Bâldea, I.; Frisbie, C. D. Work Function and Temperature Dependence of Electron Tunneling through an N-Type Perylene Diimide Molecular Junction with Isocyanide Surface Linkers. *Nanoscale* **2018**, *10*, 964−975.
(46) Cornil, D.; Li, H.; Wood, C.; Pourtois, G.; Brédas, J.-L.; Cornil, J. Work-Function Modification of Au and Ag Surfaces upon Deposition of Self-Assembled Monolayers: Influence of the Choice of the Theoretical Approach and the Thiol Decomposition Scheme. *ChemPhysChem* **2013**, *14*, 2939−2946.
(47) Quek, S. Y.; Venkataraman, L.; Choi, H. J.; Louie, S. G.; Hybertsen, M. S.; Neaton, J. B. Amine−Gold Linked Single-Molecule Circuits: Experiment and Theory. *Nano Lett.* **2007**, *7*, 3477−3482.
(48) Smith, N. V.; Chen, C. T.; Weinert, M. Distance of the Image Plane from Metal Surfaces. *Phys. Rev. B: Condens. Matter Mater. Phys.* **1989**, *40*, 7565−7573.
(49) Kaasbjerg, K.; Flensberg, K. Image Charge Effects in Single-Molecule Junctions: Breaking of Symmetries and Negative-Differential Resistance in a Benzene Single-Electron Transistor. *Phys. Rev. B: Condens. Matter Mater. Phys.* **2011**, *84*, 115457.
(50) Kitouni, R.; Selvanathan, P.; Galangau, O.; Norel, L.; Ouarda, B.; Rigaut, S. Novel Electron-Deficient Oligo(Phenyleneethynylene) Derivatives for Molecular Electronics. *Synth. Commun.* **2018**, *48*, 1052−1059.
(51) Tour, J. M.; Rawlett, A. M.; Kozaki, M.; Yao, Y.; Jagessar, R. C.; Dirk, S. M.; Price, D. W.; Reed, M. A.; Zhou, C.-W.; Chen, J.; Wang, W.; Campbell, I. Synthesis and Preliminary Testing of Molecular Wires and Devices. *Chem.—Eur. J.* **2001**, *7*, 5118−5134.
(52) Bâldea, I. Ambipolar Transition Voltage Spectroscopy: Analytical Results and Experimental Agreement. *Phys. Rev. B: Condens. Matter Mater. Phys.* **2012**, *85*, 035442.
(53) Bâldea, I.; Xie, Z.; Frisbie, C. D. Uncovering a Law of Corresponding States for Electron Tunneling in Molecular Junctions. *Nanoscale* **2015**, *7*, 10465−10471.
(54) Xie, Z.; Bâldea, I.; Oram, S.; Smith, C. E.; Frisbie, C. D. Effect of Heteroatom Substitution on Transport in Alkanedithiol-Based

https://doi.org/10.1021/acsami.1c16398
ACS Appl. Mater. Interfaces 2021, 13, 56404−56412

Molecular Tunnel Junctions: Evidence for Universal Behavior. *ACS Nano* **2017**, *11*, 569−578.
(55) Xie, Z.; Bâldea, I.; Demissie, A. T.; Smith, C. E.; Wu, Y.; Haugstad, G.; Frisbie, C. D. Exceptionally Small Statistical Variations in the Transport Properties of Metal-Molecule-Metal Junctions Composed of 80 Oligophenylene Dithiol Molecules. *J. Am. Chem. Soc.* **2017**, *139*, 5696−5699.
(56) Alloway, D. M.; Hofmann, M.; Smith, D. L.; Gruhn, N. E.; Graham, A. L.; Colorado, R.; Wysocki, V. H.; Lee, T. R.; Lee, P. A.; Armstrong, N. R. Interface Dipoles Arising from Self-Assembled Monolayers on Gold:? UV-Photoemission Studies of Alkanethiols and Partially Fluorinated Alkanethiols. *J. Phys. Chem. B* **2003**, *107*, 11690−11699.
(57) Braun, S.; Salaneck, W. R.; Fahlman, M. Energy-Level Alignment at Organic/Metal and Organic/Organic Interfaces. *Adv. Mater.* **2009**, *21*, 1450−1472.
(58) Cahen, D.; Kahn, A. Electron Energetics at Surfaces and Interfaces: Concepts and Experiments. *Adv. Mater.* **2003**, *15*, 271−277.
(59) Yaffe, O.; Qi, Y.; Scheres, L.; Puniredd, S. R.; Segev, L.; Ely, T.; Haick, H.; Zuilhof, H.; Vilan, A.; Kronik, L.; Kahn, A.; Cahen, D. Charge Transport across Metal/Molecular (Alkyl) Monolayer-Si Junctions Is Dominated by the LUMO Level. *Phys. Rev. B: Condens. Matter Mater. Phys.* **2012**, *85*, 045433.
(60) Malicki, M.; Heimel, G.; Guan, Z.-L.; Ha, S. D.; Barlow, S.; Kahn, A.; Marder, S. R. Energy-Level Alignment in 4′-Substituted Stilbene-4-thiolate Self-Assembled Monolayers on Gold. *J. Phys. Chem. C* **2011**, *115*, 7487−7495.
(61) D'Avino, G.; Muccioli, L.; Castet, F.; Poelking, C.; Andrienko, D.; Soos, Z. G.; Cornil, J.; Beljonne, D. Electrostatic Phenomena in Organic Semiconductors: Fundamentals and Implications for Photovoltaics. *J. Phys.: Condens. Matter* **2016**, *28*, 433002.
(62) Cornil, D.; Olivier, Y.; Geskin, V.; Cornil, J. Depolarization Effects in Self-Assembled Monolayers: A Quantum-Chemical Insight. *Adv. Funct. Mater.* **2007**, *17*, 1143−1148.

https://doi.org/10.1021/acsami.1c16398
ACS Appl. Mater. Interfaces 2021, 13, 56404−56412